Triplet structure in the spontaneous-emission spectrum of two coupled vertical-cavity semiconductor lasers

S. F. Pereira,* M. P. van Exter, and J. P. Woerdman
Leiden University, Huygens Laboratory, P.O. Box 9504, 2300 RA Leiden, The Netherlands
(Received 3 February 2000; published 14 September 2000)

We have measured the spectrum of the amplified spontaneous emission of two coupled vertical-cavity semiconductor lasers. The spectrum shows a triplet structure consisting of a central peak at the lasing frequency and two sidebands. Theoretical analysis shows that the sidebands are due to spatial relaxation oscillations; the triplet structure is a result of spatial hole burning which occurs due to interference between the lasing supermode and the fluctuations in the nonlasing supermode.

PACS number(s): 42.55.Sa, 42.55.Px, 42.60.Da, 42.50.Lc

Phase-locked semiconductor laser arrays are of interest as sources to produce high output power in a coherent beam and for applications in one- or two-dimensional devices. These arrays usually exhibit stable antiphase locking, i.e., all the lasers oscillate in the same frequency with each one being out-of-phase with respect to the neighboring ones. This mode is usually referred to as the antisymmetric supermode and has been experimentally observed in various semiconductor laser arrays [1–3]. Theoretically, the dominance of the out-of-phase supermode is generally explained using simple coupled-mode analysis [4,5]. However, the interaction between the optical field and the carrier density results in complex dynamics between the lasers, where the amplitude (and phase) fluctuations in one laser can lead to amplitude and phase changes in the second laser, which in turn can destabilize the phase locking between the lasers [6,7]. These theories refer to arrays of both edge emitting and vertical-cavity surface-emitting lasers (VCSELs). Presently, the interest is mainly in VCSEL arrays in view of their tremendous potential for 2D integration.

One way to investigate the dynamics of semiconductor lasers in general and semiconductor laser arrays in particular is via measurements of the spontaneous emission into the nonlasing modes. The investigation of the nonlasing modes has been a powerful tool to understand the dynamics of surface-emitting lasers. In this paper, we demonstrate experimentally predictions of the theoretical model of Hofmann and Hess [8] which relates the dynamics of two coupled VCSELs with the spectrum of the nonlasing mode. As will be shown below, this spectrum can be directly measured, and information about the coupling between the lasers can be deduced.

We first review briefly in qualitative terms the model of Hofmann and Hess [8]. The dynamic equations of the field and the carrier densities of a two-laser array are derived in terms of the symmetric and antisymmetric supermodes. This model, also referred as split-density model, redivides the carrier densities of the individual lasers into two distinct density pools. The total carrier density, i.e., the sum of the carrier densities of both lasers, interacts equally strong with both supermodes, whereas the carrier density difference of the lasers (due to spatial hole-burning effects) couples the two supermodes. The symmetric and antisymmetric supermodes, the total carrier density and the difference carrier density form a system of coupled equations whose stable solutions predict that only the antisymmetric supermode will lase. The interaction between the lasers is described via de carrier diffusion rate, the dissiptive optical coupling (i.e., additional losses in the region where the two laser field modes interfere) and the coherent coupling of the two localized fields. When small fluctuations are added around the stationary solution, the coupling of the amplitude and phase of the laser field appears in the fluctuation dynamics of the symmetric (nonlasing) mode. From analysis of the in- and out-of-phase fluctuations, it is derived that the interference between the amplified spontaneous emission of the nonlasing mode and the lasing mode causes spatial hole burning which, in a certain regime, gives rise to relaxation oscillations that phase lock amplified spontaneous emission to the laser light. This phase locking can be seen in the spectrum of the amplified spontaneous emission, i.e., in the nonlasing supermode, which has a centerline at the laser frequency and two sidebands corresponding to the relaxation oscillation frequency.

We have measured the spectrum of the symmetric nonlasing mode of a two VCSEL array for various pump parameters. The two-laser array is made by optical pumping using two pump beams which are focused on a uniform VCSEL wafer. The optical confinement in these optically pumped VCSELs is based upon a mixture of thermal index-guiding and carrier-related index and gain guiding [12,13]. Since there is no built-in guiding profile, the size of each pump spot, the pump power and the distance between the spots can be easily varied. We used these parameters to find conditions where the two lasers lock at the same frequency in the antisymmetric supermode. The distance between the lasers was made large enough to avoid the presence of lateral high-order modes [9].

Our optically pumped VCSEL wafer was grown at the CSEM Institute in Zürich. The wafer is a pin-doped 1-λ cavity of $Al_{0.18}Ga_{0.82}$ with a gain medium of three GaAs quantum wells, each 8 nm thick. The VCSEL is pumped at

*Present address: TU Delft, Optics Research Group, Lorentzweg 1, 2628 CJ, Delft, The Netherlands.

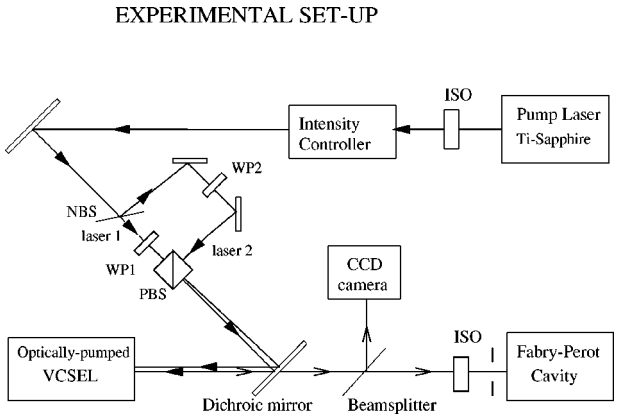

FIG. 1. Experimental set-up: Thick arrows correspond to the pump beam and thin arrows to the VCSEL beam. WP1,2: half wave plates, PBS: polarizing beam splitter, NBS: nonpolarizing 50% beam splitter, ISO: Faraday Isolator.

760 nm with a titanium-sapphire laser and emits at 850 nm. The intensity noise of the pump laser is reduced with an intensity controller which consists of a combination of an electro-optic modulator and a polarizer in an active feedback loop. The threshold power of each laser is about 42.5 mW, and the supermode is single frequency and linearly polarized. Figure 1 shows the setup used to pump the two VCSELs. By means of a nonpolarizing (NBS) and a polarizing (PBS) beam splitter the linearly polarized pump beam is split into two almost collinear beams which are focused on the VCSEL wafer by a set of lenses ($f=29$ mm). Because of the orthogonal polarizations of the two beams there can be no interference between the two pump spots. The power ratio between the two pump spots can be adjusted by means of halfwave plates WP1 and WP2. The light emitted by the VCSEL is separated from the reflected pump beam by a dichroic mirror. The VCSEL beam is then partially reflected to a CCD camera, where the near- and far-field images could be monitored by using an adjustable lens combination. The spectrum of the lasing and nonlasing modes (same polarization) are measured with a Fabry-Perot cavity (10 GHz free spectral range, resolution 0.05 GHz). The pinhole before the Fabry-Perot cavity could be spatially displaced to observe either the lasing or the nonlasing modes. Faraday isolators (ISO) were placed before the Fabry-Perot and in the pump laser path to avoid back reflection of the laser emission into the wafer and pump laser.

We observed antiphase locking between the two VCSELs when the distance between the pump spots was between 10–12 μm. When the lasers were locked in the antisymmetric mode, the near- and far-field images were as shown in Figs. 2(a) and 2(b). The two-lobed structure in the far field shows that the two lasers are out-of-phase. Simultaneous measurement of the laser spectrum shows a linearly polarized, single-frequency narrow line (linewidth FWHM $\sim$150 MHz). In contrast, we show in Figs. 2(c) and 2(d) the situation where the lasers were unlocked (reached by increasing further the distance between the pump spots); the far-field image [Fig. 2(d)] now showed no phase relation between the two lasers and the laser spectrum had two distinct

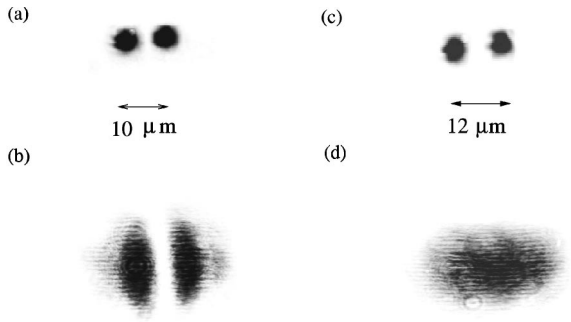

FIG. 2. (a) Near-field and (b) far-field images of the two coupled VCSELs locked in the antisymmetric supermode. (c) Near- and (d) far-field images of two VCSELs that are not locked in a supermode [each lobe of Fig. 2(c) correspond to a slight difference frequency].

peaks, each corresponding to one individual laser. At distances between the spots smaller than 10 μm, the near and far fields had lateral structure such as reported in Ref. [9]. We have also analyzed the locking of the two VCSELs as a function of the power imbalance of the pump beam. Data shows that for a power imbalance of up to 1%, the lasers were still locked.

While keeping the laser locked as in Figs. 2(a) and 2(b), we used a pinhole to spatially block the laser light (two-lobed structure) into the Fabry-Perot cavity. In this way one can distinguish the lasing from the nonlasing mode since at the region where the antisymmetric lasing mode vanishes (between the two lobes), the symmetric nonlasing mode has a maximum intensity. The main part of Fig. 3 shows the spectra of the nonlasing mode, measured at pump powers from 43 to 48 mW per VCSEL. A central peak at the laser frequency and two sidebands are clearly visible in the spec-

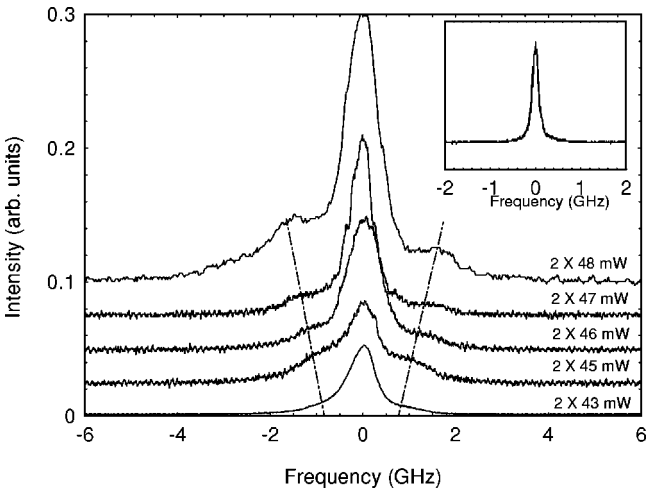

FIG. 3. Spectra of the symmetric nonlasing supermode at input pump powers of 43, 45, 46, 47, and 48 mW per VCSEL. Upper right box shows the spectrum of the lasing mode (obtained by moving the pinhole to the region of the far field where intensity is maximum) at input power of 47 mW. The laser linewidth is limited by the resolution of the Fabry-Perot cavity. The dot-dashed lines draw attention to the side bands.

tra. Note that the frequency of the sidebands increases with the pump power. We have also found that the sidebands are relatively much stronger for the nonlasing mode than for the lasing mode, as predicted in Ref. [8]. In fact, the inset of Fig. 3 shows the spectrum of the lasing mode (obtained by displacing the pinhole to the maximum intensity of the two-lobe transverse mode) at $P=47$ mW. In this spectrum, the relaxation-oscillation sidebands are too weak to be visible; careful measurement shows that they are nevertheless present, with $\sim 1\%$ of the height of the central peak. At pump powers above 48 mW, high-order transverse modes appeared.

We return now to the theoretical model of Ref. [8] in more detail than before. Linearization around the steady state of the oscillating antisymmetric supermode $(-)$ results in a 3×3 evolution matrix description for the in- and out-of-phase fluctuation amplitudes of the (nonlasing) symmetric supermode $(+)$ and the inversion difference Δ between the two lasers. Important parameters in the model are the frequency difference Ω, the gain difference s between the symmetric and antisymmetric supermode, and the carrier diffusion rate Γ between the two lasers. The relaxation oscillation frequency is given by $\omega_s=\sqrt{2\kappa_- wI_0}$, where κ_- is the cavity loss rate, and wI_0 is the normalized laser intensity, i.e., relative to the saturation intensity. In our experiment, we examined the case where the frequency difference Ω is much smaller than the relaxation oscillation frequency. In this limit the spectrum of the amplified spontaneous emission into the symmetric supermode (nonlasing mode) is a triplet consisting of a centerline at the laser frequency and two sidebands at the relaxation oscillation frequency ω_s, given explicitly by

$$I_+(\omega)=\frac{\kappa_-}{2\pi}\left[\frac{1+\alpha^2}{(s+\alpha\Omega)^2+\omega^2}\right] + \frac{\kappa_-}{2\pi}\left\{\frac{1+\alpha^2+2[\Omega+\alpha\gamma_s]/\sqrt{2\kappa_- wI_0}}{(\gamma_s-\alpha\Omega)^2+4(\omega+\sqrt{2\kappa_- wI_0})^2}\right\} + \frac{\kappa_-}{2\pi}\left\{\frac{1+\alpha^2-2[\Omega+\alpha\gamma_s]/\sqrt{2\kappa_- wI_0}}{(\gamma_s-\alpha\Omega)^2+4(\omega-\sqrt{2\kappa_- wI_0})^2}\right\}, \quad (1)$$

with

$$\gamma_s=\gamma+wI_o+2\Gamma+s, \quad (2)$$

where γ is the carrier decay rate and α is the linewidth enhancement factor $(\alpha>0)$.

For $s\ll\kappa$ the behavior of the frequency of the sidebands is identical to that of conventional relaxation oscillations; it increases with the stimulated emission rate $wI_0\approx\mu\gamma$, where $\mu=(P/P_{th}-1)$ is the output power relative to saturation. However, the damping rate behaves differently; the side bands are not only damped by spontaneous and stimulated emission $(\gamma+wI_0)$, as usual, but also by the carrier diffusion (Γ), the loss difference s, and the frequency difference Ω. The spectral width of the side bands is given by

$$\Delta\omega_s=\gamma_s-\alpha\Omega. \quad (3)$$

Furthermore, the low-frequency sideband intensity is greater than the high-frequency side band intensity. This asymmetry can be quantified by the intensity ratio of the side bands as

$$r=\frac{(1+\alpha^2)\omega_s+2(\Omega+\alpha\gamma_s)}{(1+\alpha^2)\omega_s-2(\Omega+\alpha\gamma_s)}, \quad (4)$$

Note the two contributions to r in the Eq. (3): the frequency difference Ω between the lasing and nonlasing modes and the effective damping rate γ_s (the latter is only effective via the α factor). Since in the case of our experiment, the frequency Ω is very small, the main contribution to the asymmetry of the sidebands comes from the α factor. A physical picture of this asymmetry comes from the fact that the α factor induces a change in the relative phase between the two lasers which implies coupling of the lasing and nonlasing modes. The α factor thus correlates the fluctuations that are in-phase with the laser field with the fluctuations that are out-of-phase with the laser field. Thus, not only the in-phase but also the out-of-phase fluctuations should be considered in the relaxation oscillations dynamics. This dynamics gives rise to the sidebands in the spectrum, and the nonsymmetric evolution of the in- and out-of-phase fluctuations results in the asymmetry of the side bands.

By fitting the theoretical spectrum Eq. (1) to the data of Fig. 3 we were able to determine various parameters of the system of two coupled VCSELs. We have also looked at the frequency of the side bands $\omega_s=(2\mu\kappa_-\gamma)^{1/2}$ as a function of $\mu^{1/2}=(P/P_{th}-1)^{1/2}$. By fitting these data points to a straight line we obtain $\omega_s/2\pi=4\mu^{1/2}$ GHz so that the product $\kappa_-\gamma=315$ ns^{-2}. The intensity ratio r of the sidebands [Eq. (3)] and their spectral width $\Delta\omega_s$ [Eq. (4)] are directly measured from the spectra; in the case of the highest pump power we find $r=2.4$ and $\Delta\omega_s/2\pi=1.14$ GHz. By eliminating Ω from Eqs. (3) and (4) and using the experimental values for r, ω_s, and $\Delta\omega_s$, and assuming $\alpha=4$, we obtain $\gamma_s=8.2$ ns^{-1}. The carrier diffusion rate Γ can be deduced from the ambipolar diffusion constant and the distance d between the lasers using the relation $\Gamma\sim 40$ ns$^{-1}/d^2$, with d expressed in μm [8]. Finally, taking the expression for γ_s given in Eq. (2) and using $\Gamma=40$ ns$^{-1}/100\mu$m^2 $=0.4$ ns^{-1} for the diffusion rate, we obtain $s+1.16\gamma$ $=7.4$ ns^{-1}.

As an aside we note that the same theory applies for the polarization dynamics of a single VCSEL, where one deals with two polarization degrees of freedom instead of two spatial degrees of freedom. Note, however, that in the polarization case the experiments are in the opposite regime, i.e., the relaxation oscillation is slower than the dominant relaxation rate of the medium, being in this case the spin flip rate [10,11]. Thus in the polarization case relaxation oscillation sidebands do not appear in the spectrum.

In conclusion, we have observed triplet structure in the spontaneous-emission spectrum of two coupled VCSELs. Our experimental results confirm the theoretical description [8] of spontaneous emission of coupled VCSELs. The spectrum of the nonlasing mode provides a direct and relatively

simple way to determine the degree and type of coupling in VCSEL arrays.

We would like to thank M. Moser and K. H. Gulden of the CSEM Institute in Zürich, Switzerland, for providing the VCSEL wafer. We also acknowledge support of the ''Stichting voor Fundamenteel Onderzoek de Materie (FOM)'' and of the European Union in the TMR network ERB4061 PL951021 (Microlasers and Cavity QED).

[1] M. Orenstein, E. Kapon, J.P. Harbison, L.T. Florez, and N.G. Stoffel, Appl. Phys. Lett. **60**, 1535 (1992).
[2] R.A. Morgan, K. Kojima, T. Mullally, G.D. Guth, M.W. Focht, R.E. Leibenguth, and M. Asom, Opt. Lett. **18**, 352 (1993).
[3] J.M Catchmark, L.E. Rogers, R.A. Morgan, M.T. Asom, G.D. Guth, and D.N. Christodoulides, IEEE J. Quantum Electron. **32**, 986 (1996).
[4] E. Kapon, J. Katz, and A. Yariv, Opt. Lett. **9**, 125 (1984).
[5] H.J. Yoo, J.R. Hayes, E.G. Paek, A Scherer, and Y.S. Kwon, IEEE J. Quantum Electron. **QE-26**, 1039 (1990).
[6] H.G. Winful and S.S. Wang, Appl. Phys. Lett. **53**, 1894 (1988).
[7] S.S. Wang and H.G. Winful, Appl. Phys. Lett. **52**, 1774 (1988).
[8] H. Hofmann and O. Hess., J. Opt. Soc. Am. B **16**, 137 (1999); Opt. Lett. **23**, 391 (1998).
[9] R.F.M. Hendriks, M.P. van Exter, J.P. Woerdman, and C.J. van der Poel, Appl. Phys. Lett. **69**, 869 (1996).
[10] M. San Miguel, Q. Feng, and J.V. Moloney, Phys. Rev. A **52**, 1728 (1995).
[11] M.P. van Exter, R.F.M. Hendriks, and J.P. Woerdman, Phys. Rev. A **57**, 2080 (1998).
[12] L. Raddatz, I.H. White, H.D. Summers, K.H. Hahn, M.R. Tan, and S.-Y. Wang, IEEE Photonics Technol. Lett. **8**, 743 (1996).
[13] R.F.M. Hendriks, M.B. Willemsen, M.P. van Exter, and J.P. Woerdman, Opt. Commun. **149**, 50 (1998).